J Mater Sci: Mater Electron (2017) 28:16348–16357
DOI 10.1007/s10854-017-7542-x

Influence of dopant on structural, optical and dielectric properties of $Sn_{1-X}Co_xO_2$ nanoparticles

M. P. Rajeeva[1] · C. S. Naveen[2] · Ashok R. Lamani[1] · H. S. Jayanna[1]

Received: 23 May 2017 / Accepted: 14 July 2017 / Published online: 20 July 2017

Abstract In this work, the optical and dielectric properties of Co doped SnO_2 nanoparticles were studied using a.c. impedance spectroscopy. X-ray diffraction (XRD) confirmed that the Co doped SnO_2 powder samples have the same tetragonal structure as pure SnO_2 nanoparticles. The structural, surface morphological studies, compositional analyses and optical energy band gap were investigated by XRD, Scanning electron microscopy (SEM), Energy Dispersive X-ray Analysis (EDAX), and UV–Vis Spectroscopy. It is evident from the XRD result that annealed SnO_2 samples exhibits tetragonal crystal structure with crystallite size ranging from 8 to 12 nm. The optical band gaps value of doped SnO_2 nanoparticles were calculated to be in the range 5.33–5.8 eV. Impedance spectroscopy was carried out at room temperature in the frequency range of 100 kHz–14 MHz to explore the electrical properties of $Sn_{1-x}Co_xO_2$ nanoparticles. For all the Co doped SnO_2 samples prepared with Co content $x \leq 0.04$, the SnO_2 lattice contracts with the increasing dopant concentration. The dielectric constant, dielectric loss and a.c. electrical conductivity decrease with the increase in Co doping concentration. The decrease of dielectric constant and dielectric loss of the nanomaterial with respect to increasing frequency suggests that this nanomaterial can be employed in the fabrication of devices used at high-frequencies.

✉ H. S. Jayanna
jayanna60@gmail.com

[1] Department of P.G studies and Research in Physics, Kuvempu University, Jnanasahyadri, Shankarghatta, Shimoga, Karnataka 577451, India

[2] Department of Physics, Alliance College of engineering and design, Alliance University, Anekal, Bengaluru 562106, India

1 Introduction

Tin dioxide (SnO_2) presents special properties such as remarkable chemical and thermal stabilities, high transparency in the visible spectral range and low electrical resistivity [1, 2] with direct applications for photodetectors, solar cells, liquid crystal displays and transparent conducting electrodes. In addition, this material has shown its importance as a gas and humidity sensor due to the strong conductivity changes produced by chemisorbed gas molecules on its surface [3–5]. The coexistence of tin interstitials and oxygen vacancies in SnO_2, gives the unique combination of transport and optical properties [6]. More recently, SnO_2nanocrystalline material has received a growing attention due to its excellent properties arising out of large surface to volume ratio, quantum confinement effect, etc. [7–10].

Morphology, size of SnO_2 nanoparticles and its distribution plays an important role in deciding their properties. However, one important method to tailor the properties of the nanoparticles is by introducing the dopant in the host system. The appropriate dopants are often used in the SnO_2 matrix, which modify its microstructure and defect chemistry, resulting in a change in its electrical and optical properties. Doping the SnO_2 nanostructures with metals and metal oxides without altering the optical transparency is the primary means of controlling electrical conductivity which makes it as an important component for optoelectronic applications. The 3d transition metal ions as dopants with open d-shell electronic configurations have various unique physical properties including magnetic ground states that make them attractive for altering the magnetic, photoluminescence or other physical properties of their host semiconductors [11, 12].

Size-dependent properties are the most essential aspects to explore the novel characteristics of the materials. In particular, the electrical properties of nanoscaled materials have attracted much interest in recent years because of their unique size-dependent nature. Moreover, the grain property and grain boundary effects lead to the variation of conducting nature in materials [13, 14]. Impedance spectroscopy is one of the essential tools to study the electrical properties of a material as a function of frequency.

Many methods have been employed to produce SnO_2 nanoparticles. Among all the gel combustion method is facile as it demands less costly equipment and hence the preparation procedure is simple and cost effective. The reaction is environmentally friendly since by-products are CO_2, N_2, Cl_2, O_2 and H_2O. It is a safe and quick reaction completes within 15 min. By adopting the above discussed technique, we have synthesized cobalt doped tin oxide nanoparticles with different size by varying the dopant concentration during synthesis as nowadays applications require a high surface area and controlled defects which determine the optical and electrical properties [14]. There are many reports [15–17] on the electrical property of transition metal doped SnO_2 nanomaterials. However, to the best of our knowledge there are less research articles available on a.c. electrical properties of Co doped SnO_2, therefore it is essential to study the same.

In the present work, we report the synthesis of pure and Co doped SnO_2 nanoparticles using gel combustion method. The prepared samples were characterized to investigate their structural, morphological, a.c. conductivity, and dielectric properties at the nanoscale as a function of frequency and cobalt concentration.

2 Experimental

$Sn_{1-x}Co_xO_2$ (x = 0, 0.01, 0.02, 0.03, 0.04) were prepared by gel combustion method. The raw materials used are Tin(II) chloride dihydrate ($SnCl_2.2H_2O$, 99.99 + %, Merck),$CoCl_2.6H_2O$ (99.99 + %, Merck) and Nitric acid (HNO_3, 70 + %, Merck). These raw materials were dissolved in distilled water and mixed in an appropriate ratio to form a tin nitrate solution. Then Citric acid, which acts as fuel ($C_6H_8O_7$, 99.5%, Merck) was added to this solution. The solution was heated with constant stirring to a temperature about 90 °C in a beaker and then the concentration of the solution slowly became higher, eventually a polymeric precursor was formed. Further, when the temperature was raised to 300 °C, the polymeric precursor went through a strong, self-sustained combustion reaction with an evolution of large volume of gases and swelled into voluminous and foamy ashes. The entire combustion process has been completed in a few minutes. The resulting ashes were then calcined at 800 °C until complete decomposition of the carbonaceous residues was achieved and the chemical reaction equation is as follows [18],

$$SnCl_2{\cdot}2H_2O + (1-x)CoCl_2{\cdot}6H_2O + 6.2HNO_3 + 1.5C_6H_8O \rightarrow Sn_{1-x}Co_xO_2 + xCl_2 + 3.1N_2 + \left(6+\frac{x}{2}\right)H_2O + 9CO_2 + \left(\frac{5x}{2}-\frac{31}{4}\right)O_2$$

The obtained SnO_2 powder was made into pellets of 12 mm diameter and around 1.5 mm thickness by uniaxial pressing, followed by cold isostatic pressing at a pressure of 20 MPa. These disc shaped samples were used to measure the dielectric parameters.

The crystal structure of $Sn_{1-x}Co_xO_2$ was analyzed by XRD method using Cu-K_α radiation ($\lambda = 1.5418$ Å) operating at 30 kV and 15 mA. The scan rate was 5°/min and the range was between 20° and 80°. The average crystallite size was calculated by observing and calculating the X-ray line broadening using the Scherrer's relation,

$$d = \frac{0.89\lambda}{\beta\cos\theta} \quad (1)$$

where, 'λ' the wavelength of X-ray used and 'β' the full width at half maximum (FWHM), K = 0.89 the Scherrer's constant value for spherical crystallites and 'θ' the Bragg angle.

The surface morphology and shape of the nanoparticles of powdered samples were investigated by SEM (Hitachi Model S-3200N).The elemental analyses of the powdered samples were carried out by using EDAX spectra. The dielectric behaviour and a.c. conductivity (σ_{ac}) of $Sn_{1-x}Co_xO_2$in the frequency range from 100 KHz to15 MHz were carried out by using an LCR meter (N4L: PSM1735).

3 Results and discussion

3.1 X-ray diffraction (XRD) measurement

Figure 1 shows the X-ray powder diffraction patterns of $Sn_{1-x}Co_xO_2$ nanocrystallites. All the diffraction peaks are well assigned to the tetragonal system of SnO_2 with a standard reference pattern (JCPDS # 41-1445) and on doping with cobalt a similar pattern was observed except that the diffraction peak shifts slightly to the higher angle in comparison to pure SnO_2. No extra diffraction peaks from Co or other impurities were detected. It is also observed that the FWHM of the diffraction peaks increases with increasing Co content in the specimens. The decrease in FWHM along with an increase in peak intensity suggests that, by incorporation of dopant into

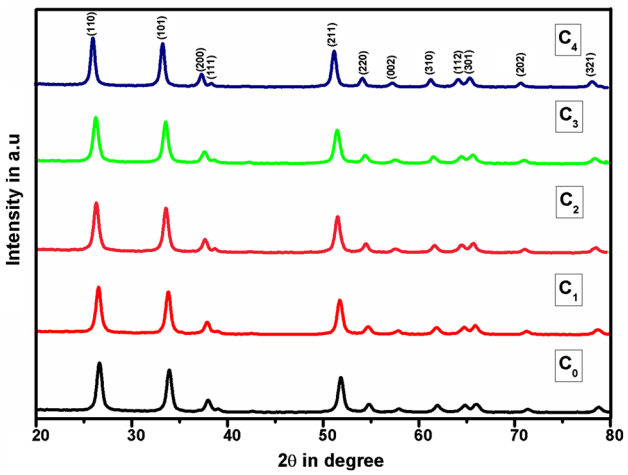

Fig. 1 XRD Pattern of $Sn_{1-x}Co_xO_2$ nanoparticles

the SnO_2 lattice results decrease in grains size of doped nanoparticles. The tetragonal distortion (c/a) ratio 0.671, 0.669, 0.667 and 0.678, respectively, calculated for SnO_2 (C_0), $Sn_{0.99}Co_{0.01}O_2$ (C_1), $Sn_{0.98}Co_{0.02}O_2$ (C_2), $Sn_{0.97}Co_{0.03}O_2$ (C_3) and $Sn_{0.96}Co_{0.04}O_2$ (C_4) samples. The decrement in the values of average crystallite size with Co doping is because of the smaller ionic radii of Co^{2+} (0.79 Å) ion thanSn^{4+} (0.83 Å) ion [19]. On doping, as the metal oxide ions occupy the regular lattice site of SnO_2, the interference takes place between Co doped metal ions and those of SnO_2 lattice, due to the crystalline behaviour of the doped metal oxides of SnO_2nanocrystallites, the average grains size tends to reduce than that of pure SnO_2 nanostructures. The average crystallite size of SnO_2 and Co doped SnO_2 nanoparticles were estimated in the range of 8–12 nm by Scherrer's method [20], and the values are tabulated in Table 1. Lattice parameter values were determined by the least square fit method. A slight variation in the unit cell parameters is observed with the increase of dopant concentration, which indeed indicates that the doped atoms might substituted into the lattice sites of parent atoms.

3.2 Scanning electron microscope (SEM)

The SEM images of the pure SnO_2 sample and those doped with 1, 2, 3 and 4% Cobalt are presented in Fig. 2. It is confirmed from the Fig. 2(C_0) that, prepared samples have particles with spherical shape and monosize dispersion of throughout the sample. It is also observed that, the porosity of the prepared samples decreases with the increasing Co concentration in SnO_2 host matrix.

3.3 Energy dispersive analysis X-ray spectroscope (EDAX)

Figure 3a–e shows the EDAX spectra, collected from the average scanned area, of C_0, C_1, C_2, C_3 and C_4 samples respectively. The self-generated elemental composition (at. wt.%) details are also presented in the Fig. 3. It is clear from the figure that Sn, and O are only the main elemental species in a pure SnO_2 sample while additionally Co peaks were observed in Co doped samples. However, C peaks, very close to the O peaks, were also appeared in all the samples. These C peaks were eliminated from the EDAX spectra, during the data analysis, to better examine the O peaks in the spectra. The atomic percentages of Co as obtained from EDAX are very close to the calculated compositions as in Table 1.

3.4 UV visible analysis

Inset of Fig. 4 shows the optical absorbance spectra of $Sn_{1-x}Co_xO_2$ samples at the near band edge region. In general absorbance of SnO_2 sample was lower due to the low excitation of an electron from the valence band to the conduction band. As in the figure, the absorbance of samples increased when the Co doping level increased from 0 to 4 mol% because the reflection and transmittance decreased in this range. The band gaps of the nanoparticles were determined from the well-known Tauc relation given by,

$$\alpha h\upsilon = A(h\upsilon - E_g)^n \quad (2)$$

where $\alpha = A/t$ is called the absorption coefficient, A is the absorbance, t is a thickness of the pellet of the powdered

Table 1 Values of EDAX data, Crystallite size, tan δ, ε', ε'' and σ_{ac} of $Sn_{1-x}Co_xO_2$ nanoparticles

Sample	Co (x)	Atomic percentage obtained from EDAX		Crystallite size (nm)	5 MHz				E_g (eV)
		Sn	Co		tan δ	ε'	ε''	$\sigma_{ac}(\Omega m)^{-1}$	
C_0	0.00	100.00	0.00	12	50.18	50.18	1.02	2.56E−4	5.33
C_1	0.01	98.94	1.06	11	46.30	46.30	0.57	1.43E−4	5.38
C_2	0.02	97.92	2.08	10.6	41.39	41.39	0.28	6.87E−5	5.43
C_3	0.03	96.89	3.11	9	38.54	38.54	0.06	1.30E−5	5.66
C_4	0.04	95.87	4.13	8.1	32.62	34.58	0.01	1.31E−6	5.80

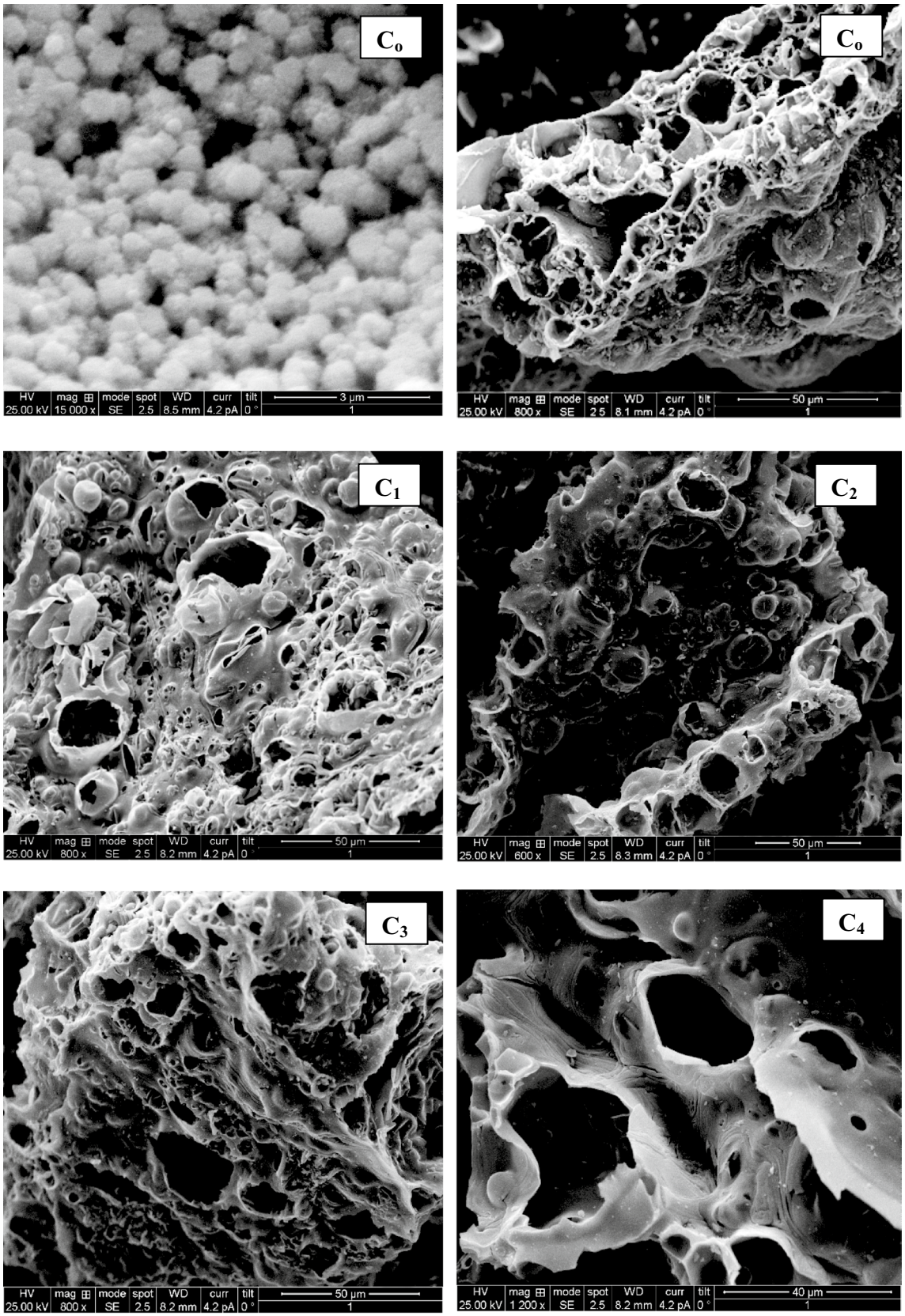

Fig. 2 SEM images of $Sn_{1-x}Co_xO_2$ samples

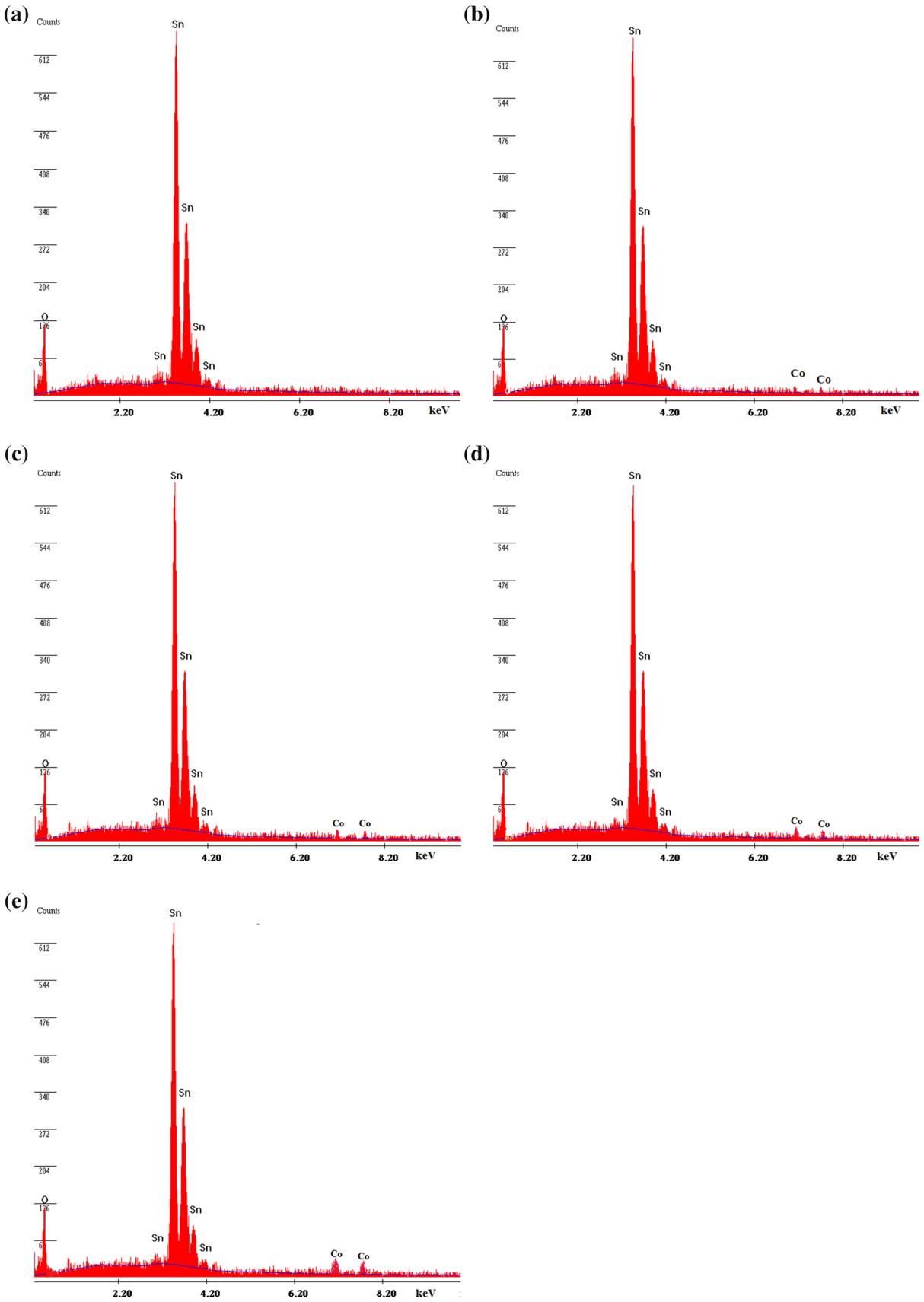

Fig. 3 EDAX patterns of **a** SnO_2, **b** $Sn_{0.99}Co_{0.01}O_2$, **c** $Sn_{0.98}Co_{0.02}O_2$, **d** $Sn_{0.97}Co_{0.03}O_2$, and **e** $Sn_{0.96}Co_{0.04}O_2$ samples

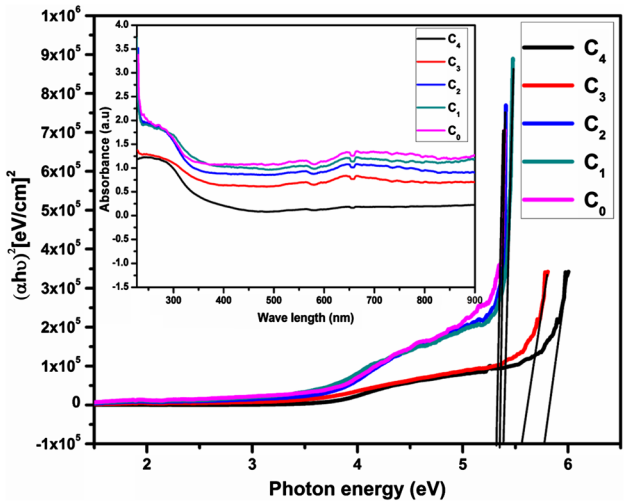

Fig. 4 Tauc plot of $Sn_{1-x}Co_xO_2$ samples

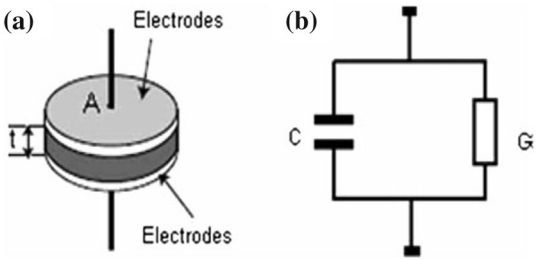

Fig. 5 **a** Capacitor formed using Kelvin fixture. **b** Equivalent circuit of Kevin fixture

sample, E_g is the band gap and n = 1/2 for direct band gap semiconductor.

The band gaps showed in Fig. 4 are tabulated as in the Table 1. The data of this study showed Co doping also has an influence on the direct optical band gap of $Sn_{1-x}Co_xO_2$ samples. It should be noted that enhancement in energy band gap ($E_g \geq 3.6$ eV) was observed after Co doping($0.00 \leq x \geq 0.04$) due to the reduction of crystallite size with the increase of dopant concentration, which is consistent with the energy band gap of various Co doped SnO_2.

3.5 Dielectric measurements

The real (ε') and imaginary (ε'') part of the permittivity can be calculated from the capacitance (C) and loss tangent ($\tan\delta$) respectively. Since the capacitor formed using Kelvin fixture Fig. 5a has a small capacity due to its large impedance, the equivalent circuit of the capacitor is considered to comprise an equivalent parallel capacitance (C) and an equivalent parallel conductance (G) as shown in Fig. 5b.

The admittance (Y) and the complex admittance (Y*) of a circuit in Fig. 5b can be expressed as:

$$Y = j\omega c = j\omega|\varepsilon|C_0 \tag{3}$$

$$Y * = G + j\omega C = j\omega\left(\frac{C}{C_0} - j\frac{G}{\omega C_o}\right)C_o \tag{4}$$

where C_o is the air capacitance and ω is the angular frequency. Therefore, the complex relative permittivity can be defined as

$$\varepsilon^* = \varepsilon' - j\varepsilon'' \tag{5}$$

and calculated by

$$\varepsilon' = \frac{C}{C_0} = \frac{tC}{\varepsilon_0 A} \tag{6}$$

$$\varepsilon'' = \varepsilon' \tan\delta \tag{7}$$

where C is the capacitance, t is the thickness and A is the cross-sectional area of the sample. The loss tangent or tan d is defined as the ratio of the imaginary part of the dielectric constant to the real part.

$$\tan\delta = \frac{\varepsilon''}{\varepsilon'} \tag{8}$$

The a.c. electrical conductivity of sample was calculated using the relation

$$\sigma_{ac} = 2\pi f \varepsilon' \varepsilon_0 \tan\delta \tag{9}$$

where 'f' is the frequency of the applied field.

Errors of the Kelvin fixture include those due to edge capacitance on the edge electrodes (stray capacitance), residual parameters of the Kelvin fixture, such as electrical length, residual impedance, stray admittance, and air gaps caused when sandwiching the sample between the electrodes. Errors due to the residual parameters of the test fixture were effectively minimized by performing ''Open,'' ''Short,'' and known ''Load'' calibrations on the sample contact using various standard resistance test fixtures of 5, 50 Ω, 5, 500 kΩ [21]. Gold electrodes were used to minimize errors due to air gaps [22].

Figure 6 shows the frequency dependence of dielectric constant at room temperature for the pure and Co-doped SnO_2samples annealed at 800 °C. In order to measure the capacitance, dielectric loss, and a.c. conductivity as a function of frequency, the circularly shaped pellets are prepared by pressing the powder into a pellet using a pellet presser with 10 mm in diameter. Gold glue electrodes are used to measure the capacitance of the cylinders (Diameter = 10 mm) with gold electrodes.

It can be seen from Fig. 6 that the dielectric constant values of the prepared samples decrease with the increase of frequency ($f \geq 100$ kHz) and becomes almost constant

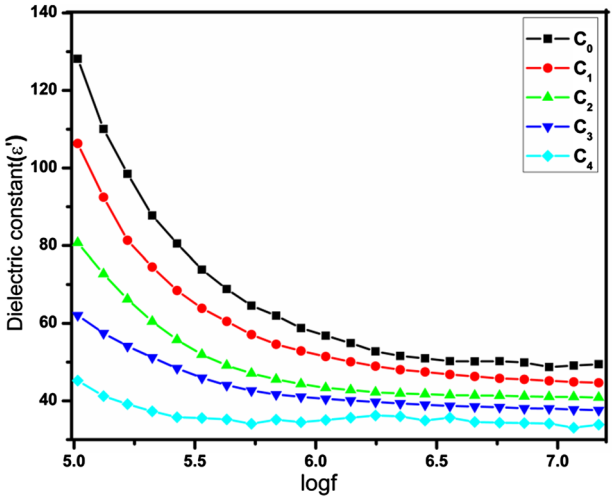

Fig. 6 $\varepsilon'$of $Sn_{1-x}Co_xO_2$ nanoparticle as a function of frequency at room temperature

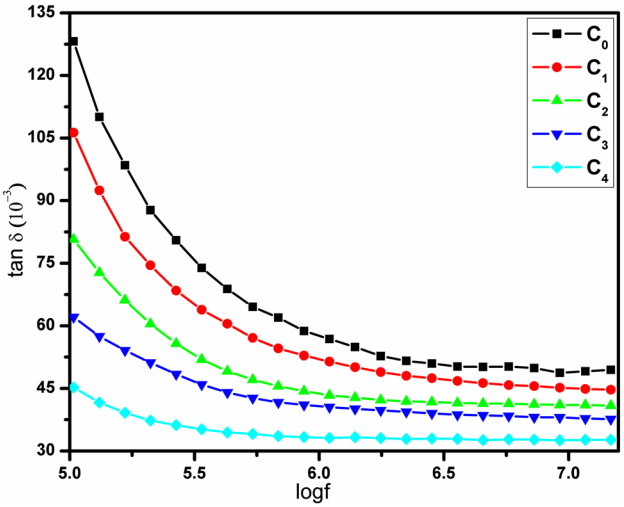

Fig. 7 $\tan\delta$ of $Sn_{1-x}Co_xO_2$ nanoparticle as a function of frequency at room temperature

at high frequencies (4 MHz ≤ f ≥ 14 MHz). This behaviour can be explained using Maxwell–Wagner interfacial model. According to this model, a dielectric medium is considered to be composed of double layers, well-conducting grains which are separated by poorly conducting or resistive grain boundaries. Under the application of the external electric field, the charge carriers can easily migrate the grains but are accumulated at the grain boundaries. This process can produce large polarization and high dielectric constant. The higher value of a dielectric constant can also be explained on the basis of interfacial/space charge polarization due to an inhomogeneous dielectric structure. The inhomogeneity present in the system may be porosity and grain structure. The polarization decreases with the increase in frequency and then reaches a constant value due to the fact that beyond a certain frequency of external field the hopping between different metal ions (Sn^{4+} and Co^{2+}) cannot follow the alternating field [23].

The dielectric loss arises when the polarization lags behind the applied a.c. field and is caused by the impurities and imperfections in the crystal lattice. The frequency dependences of $\tan\delta$ and ε'' at room temperature are shown in the Figs. 7 and 8, respectively. It is observed that the values of $\varepsilon''$and $\tan\delta$ decreases from100 kHz to 4 MHz, and thereafter (4 MHz ≤ f ≥ 14 MHz) it remains constant for all the samples, which may be attributed due to Debye relaxation mechanism. The decrease of dielectric loss ($\tan\delta$ and ε'') with the increase in frequency is may be due to the interfacial or space charge polarization effect. In other words, the dielectric loss is inversely proportional to the frequency that causes a reduction of dielectric loss with the increase in frequency [24]. At higher frequencies, the prepared materials exhibit constant and low dielectric loss values, this suggests that these samples possess a less loss nature at this frequency range. Hence these nanomaterials can be employed in the fabrication of devices used at high-frequencies (4 MHz ≤ f ≥ 14 MHz), because these devices need a constant with low energy dissipating dielectric materials.

Figures 9, 10, 11 show variation of ε',$\tan\delta$ andε'' with Co concentration in SnO_2 respectively. As depicted in the Fig. 8, one can be observed the decrease of dielectric constant from 50.18 to 34.58 with the increase of Co concentration from 0 to 4 at.wt.% at 5 MHz respectively. It may be due to the small dielectric polarizability of Co ion as compared to Tin ion. Hence, as the dopant

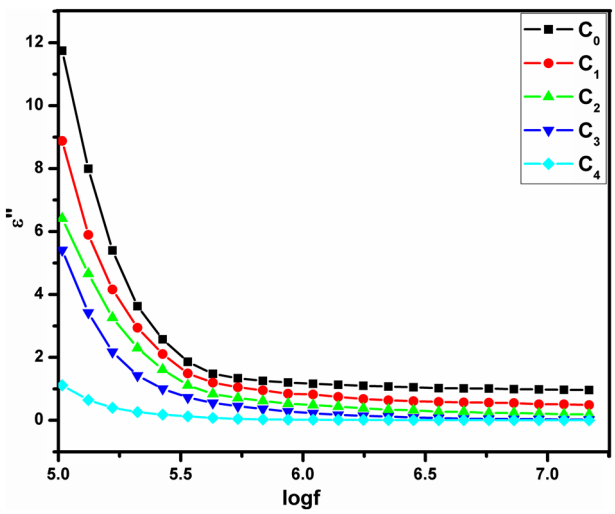

Fig. 8 ε'' of $Sn_{1-x}Co_xO_2$ nanoparticle as a function of frequency at room temperature

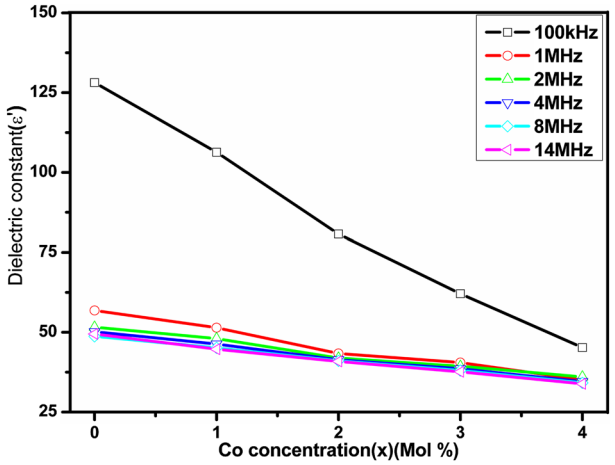

Fig. 9 Variation of ε' of $Sn_{1-x}Co_xO_2$ nanoparticles with Co concentration

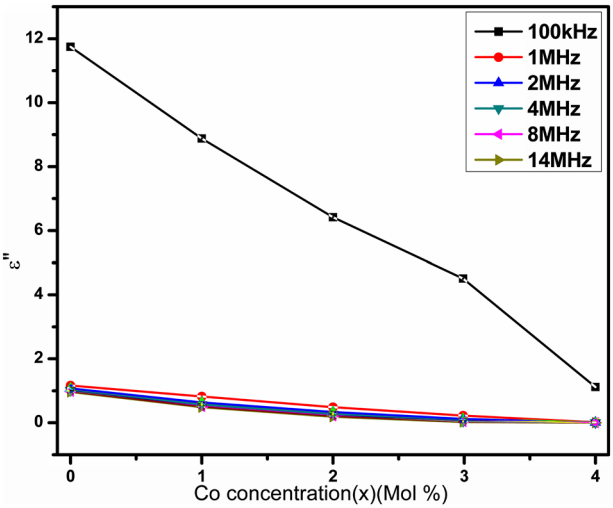

Fig. 11 ε'' of $Sn_{1-x}Co_xO_2$ nanoparticles as a function Co concentration

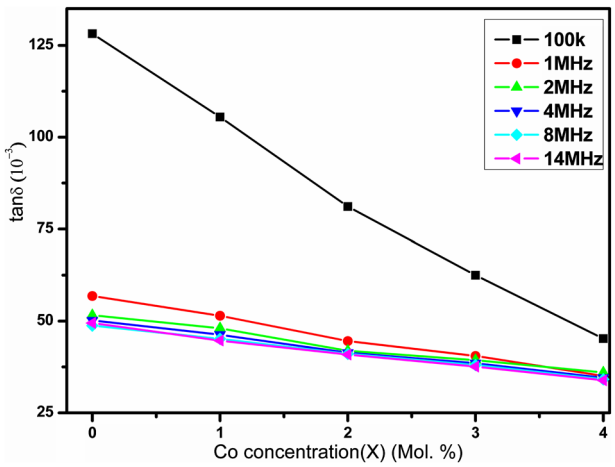

Fig. 10 $\tan\delta$ of $Sn_{1-x}Co_xO_2$ nanoparticles as a function Co concentration

concentration increases more tin ions will be substituted by the dopant ions and thereby, decreasing the dielectric polarization, which in turn decreases the dielectric constant. However, the density of a material also plays an important role in the variation of dielectric constant and dielectric losses [25]. It can also be seen that dielectric losses decrease with the increase in dopant concentration as in the Figs. 10 and 11 and become minimum in the high-frequency region which shows the capability of these materials to be used in the fabrication of devices used at high-frequencies. None of the samples show the loss peak. The peaking behaviour occurs when the hopping frequency of metal ions is equal to the frequency of applied a.c. field [26].

3.6 a.c. electrical conductivity

The a.c.conductivity increases with the increase in frequency for all compositions. Total conductivity of the system is given by

$$\sigma = \sigma_o(T) + \sigma_{ac}(\omega, T) \tag{10}$$

Here, the first term on R.H.S is dc conductivity which is independent of frequency. The second term is pure a.c. conductivity due to the electron hopping between the metal ions. The a.c. electrical conductivity (σ_{ac}) of the dielectric material can be represented by the following equation,

$$\sigma_{ac} = \varepsilon_o \varepsilon'' \omega \tag{11}$$

where ω is the angular frequency and ε_o is permittivity of free space.

As in Fig. 12, the a.c. conductivity gradually increases with the increase in the frequency of applied a.c. field. This kind of behaviour shows that it must be related to the bound carriers trapped in the sample, or due to a gradual decrease in series resistance with increasing frequency [27, 28]. Frequency dependence of the a.c. conductivity resembles that of hopping type conduction. Hopping of charge carries among the trap levels situated in the band gap of the material may give rise to frequency dependent a.c. conductivity according to the following relation,

$$\sigma_{ac} = A\omega^n; 0 < n < 1 \tag{12}$$

where A is a constant of proportionality and n is an index that depends on both the temperature and the frequency. Two other possible explanations may be attributed to the increase in conductivity. The first one is the electric energy associated with the high a.c. frequency. This can

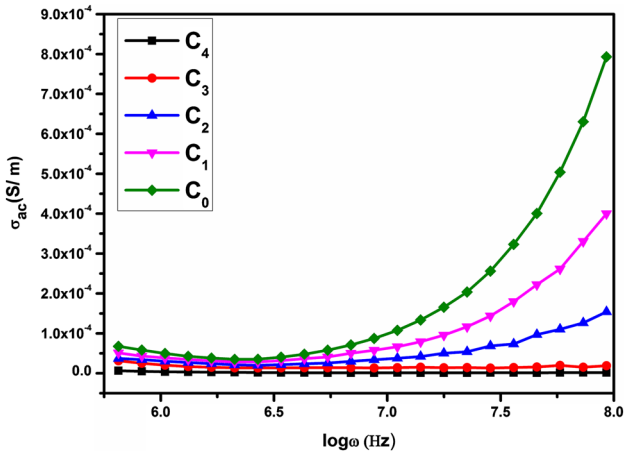

Fig. 12 Variation of a.c. conductivity of $Sn_{1-x}Co_xO_2$ nanoparticles as a function frequency

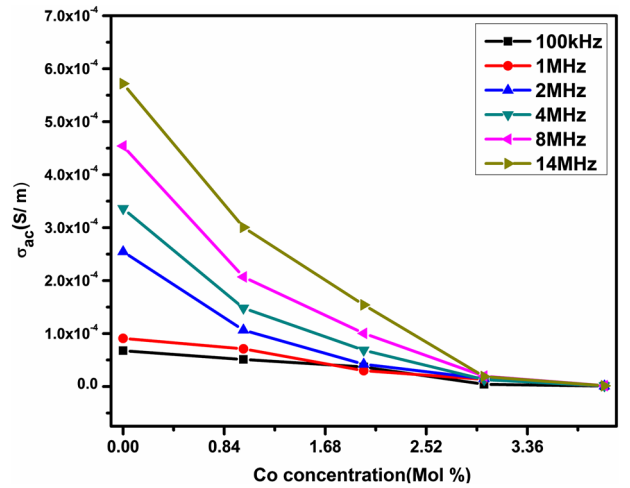

Fig. 13 Variation of a.c. conductivity of $Sn_{1-x}Co_xO_2$ nanoparticles as a Co concentration

effectively encourage the electric charge to jump between the nano-size particles. The second possible explanation could be attributed to the enhanced dielectric relaxation of the polarization of the SnO_2 nanoparticles in a high-frequency region [29, 30]. It can also be observed from the Fig. 13 that, there is a decrease of a.c. conductivity (from 2.56×10^{-4} to 1.31×10^{-6} S/m at 5 MHz) with the increase of Co concentration from 0 to 4%. It may be attributed to the fact that the Co^{+2} introduce the defect ions in SnO_2 system. These defects tend to segregate at the grain boundaries due to the diffusion process resulting from sintering and cooling processes. However, the substitution of Sn ions with Co ions can take place up to a certain limit. Thus, the increase in dopant concentration of Co the defect ions also increased and which facilities the blockage of flow of charge carriers. This is the reason for turn decreases the conductivity of the system [31].

4 Conclusions

$Sn_{1-x}Co_xO_2$ nanoparticles have been successfully prepared by the gel combustion method. The XRD patterns exhibit the tetragonal rutile structure of SnO_2 for all the samples with no impurity phase. The atomic percentages of Co dopant were confirmed from EDAX data. From UV analysis, it was found that cobalt doping enhances the optical energy band gap (E_g) of tin oxide nanoparticles. This paper also presents the research pertaining to the frequency dependence of dielectric parameters of $Sn_{1-x}Co_xO_2$ nanomaterial, which have been studied in detail across a wide frequency ranging between 100 kHz and 14 MHz at room temperature. From this study, it was analyzed and concluded that, dielectric constant, dielectric losses and a.c conductivity decrease with the increase of Co concentration ($0 \leq x \geq 0.04$). The decrease of dielectric constant and dielectric loss of the nanomaterial with respect to increasing frequency suggests that this nanomaterial can be employed in the fabrication of devices used at high-frequencies.

Acknowledgements The authors would like to acknowledge their sincere thanks to Dr. R. Somashekhar, Department of Physics, Manasagangotri, University of Mysore for providing XRD facility and Department of Material Engineering, Indian Institute of Science, Bangalore for the EDAX and SEM facilities.

References

1. J.T. Hu, M. Ouyang, P.D. Yang, C.M. Lieber, Nature **48**, 399 (1999)
2. B. Sathyaseelan, K. Senthilnathan, T. Alagesan, R. Jayavel, K. Sivakumar, Mater. Chem. Phys. **124**, 1046 (2010)
3. J. Kappler, A. Tomescu, N. Barsan, V. Weimar, Thin Solid Films **391**, 186 (2001)
4. R.K. Mishra, P.P. Sahay, Ceram. Int. **38**, 2295 (2012)
5. G. Zhang, M. Liu, Sens. Actuators B **69**, 144 (2000)
6. M. Batzill, U. Diebold, Prog. Surf. Sci. **79**, 47 (2005)
7. H.C. Chiu, C.S. Yeh, J. Phys. Chem. C **11**, 7256 (2007)
8. T.P. Hülser, H. Wiggers, F.E. Kruis, A. Lorke, Sens. Actuators B **109**, 13 (2005)
9. A. Azam, A.S. Ahmed, M.S. Ansari, M. Shafeeq, A.H. Naqvi, J. Alloys Compd. **506**, 237 (2010)
10. V. Golovanov, A.M. Matti, Sens. Actuators B Chem. **106**, 563 (2005)
11. H. Kimura, T. Fukumura, M. Kawasaki, K. Inaba, T. Hasegawa, H. Koinuma, Appl. Phys. Lett. **80**, 94 (2002)
12. R Maity, S Kundoo, K.K. Chattopadhyay, Mater. Manuf. Process. **21**, 644 (2006)
13. R Rai, T.D. Senguttuvan, S.T. Lakshmikumar, Comput. Mat. Sci. **37**, 15 (2006)
14. A.E. Owen, in *Progress in Ceramic Science. 3*, ed. by J. E. Burke, (Macmillan, New York, 1963), p. 77

15. B. Stjerna, E. Olssonand, C.G. Granqvist, J. Appl. Phys. **76**, 3797 (1994)
16. E. Shanthi, V. Dutta, A. Banerjeeand, K.L. Chopra, J. Appl. Phys. **51**, 6243 (1980)
17. E. Shanthi, A. Banerjee, V. Duttaand, K.L. Chopra, J. Appl. Phys. **53**, 1615 (1982)
18. J. H. Kang, Y. Kim, D. Young, Electrochem. Soc. **152**(3), 33 (2005)
19. N.F. Habubi, G.H. Mohamed, S.F. Oboudi, S.S. Chiad, PCAIJ **9**(5), 169 (2014)
20. V. Golovanov, A.M. Matti, Sens. Actuators. B **106**, 563 (2005)
21. Newtons 4th Ltd., Frequency response analyzer, guide to PSM1735—IAI compensation, guide to IAI calibration (2008)
22. L.B. Kong, Z.W. Li, G.Q. Lin, Y.B. Gan, Acta Mater. **55**, 6561 (2007)
23. T. Prodromakis, C. Papavassiliou, Appl. Surf. Sci. **255**, 6989 (2009)
24. H. Young, Y. Lin, H. Wang, F. Luo, Mater. Manuf. Process. **23**, 489 (2008)
25. R.V. Mangalaraja, P. Manohar, F.D. Gnanam, J. Mater. Sci. **39**, 2037 (2004)
26. R. Khan, Zulfiqar, S. Fashu, M.U. Rahman, J. Mater. Sci. **27**, 7725 (2016)
27. A. Tataroglu, S. Altındal, M.M. Bulbul, Microelectron. Eng. **81**, 140 (2005)
28. H. MahmoudiChenari, M.M. Golzan, H. Sedghi, A. Hassanzadeh, M. Talebian, Curr. Appl. Phys. **11**, 1071 (2011)
29. V.V. Daniel, *Dielectric Relaxation*, (Academic Press, London, 1967)
30. K.G. Dhinakar, T. Selvalakshmi, S.M. Sundar, A.C. Bose, J. Mater. Sci. **27**, 5818 (2016)
31. A. Azam, A.S. Ahmed, M. Chaman, A.H. Naqvi, J. Appl. Phys. **108**, 094329 (2010)